Chemical Engineering Journal 410 (2021) 127616

Contents lists available at ScienceDirect

Chemical Engineering Journal

journal homepage: www.elsevier.com/locate/cej

Biodegradable metal-derived magnesium and sodium enhances bone regeneration by angiogenesis aided osteogenesis and regulated biological apatite formation

Yang Liu [a,d,1], Huafang Li [b,c,1], Jiankun Xu [b,1], Jessica TerBush [e], Wenting Li [a], Mohan Setty [f], Shaokang Guan [g], Thanh D. Nguyen [d,h], Ling Qin [b,*], Yufeng Zheng [a,*]

[a] Department of Materials Science and Engineering, College of Engineering, Peking University, Beijing 100871, China
[b] Musculoskeletal Research Laboratory of Department of Orthopaedics & Traumatology and Innovative Orthopaedic Biomaterial and Drug Translational Research Laboratory of Li Ka Shing Institute of Health Sciences, The Chinese University of Hong Kong, Hong Kong Special Administrative Region, China
[c] School of Materials Science and Engineering, University of Science and Technology Beijing, Beijing 100083, China
[d] Department of Mechanical Engineering, Univeristy of Connecticut, Storrs, CT 06269, USA
[e] Department of Materials Engineering, Monash University, Clayton, VIC 3168, Australia
[f] Institute for Frontier Materials, Deakin University, Geelong, VIC 3216, Australia
[g] School of Materials Science and Engineering, Zhengzhou University, Zhengzhou 455001, China
[h] Department of Biomedical Engineering, Univeristy of Connecticut, Storrs, CT 06269, USA

ARTICLE INFO

Keywords:
Biodegradable metals
Magnesium alloy
Sodium
Osteogenesis
Calvarial defect

ABSTRACT

Biodegradable metals have great attraction to become orthopaedic implants. Here, we demonstrated a biodegradable magnesium alloy incorporated with essential element sodium through Sn-Na master alloying technique. The designed MgSnZnNa alloy presented better hardness and corrosion resistance due to the uniform distribution of Na in Mg_2Sn second phase and solid soluble Zn in Mg matrix. The co-release of Mg and Na ions resulted in advanced upregulation of osterix and osteocalcin expression in adipose derived stem cells *in vitro*. It significantly promoted the rat calvarial defect bone regeneration through osteogenesis and angiogenesis, attributed to the co-release of Na and Mg ions, by increasing the expression of calcitonin gene-related peptide, osteocalcin as well as vascular endothelial growth factor. The current study provided an innovative approach by using master alloy to incorporate essential elements (such as Na or K) for fabricating biodegradable Mg alloys with reduced galvanic corrosion and enhanced biological functions.

1. Introduction

Biodegradable magnesium (Mg) alloys have attracted great attention in research and development (R&D) of medical implants in the past decades because of their biodegradability and biocompatibility [1,2]. Significant milestones include but are not limited to mechanism explanatory of calcitonin gene-related peptide (CGRP) involved in Mg^{2+}-induced osteogenesis [3], commercial products in terms of bone screws [4,5] and coronary stents [6], through translational progress and clinical trials [7,8], as well as better understanding of the corrosion behavior of Mg-based biodegradable metals [9–11]. Despite the progress made for commercial products, concerns remain regarding the uncertainty of chronic toxicity in either aluminum and/or rare earth metals that are widely used in Mg-based biodegradable metals, in which these elements aid corrosion resistance of alloys both *in vitro* and *in vivo* [12,13].

Alkali elements (such as K and Na) which are essential elements in human body possess the potential as alloying elements for design of new biodegradable Mg alloys [1]. Especially, Na (Sodium) accounts for 0.2 wt% in adult body weight with 40%-45% of it in skeletons. It is involved in multiple metabolic functions, including maintaining fluid electrolyte balance, osmotic pressure balance and acid-base balance, cardiomyocyte excitability, blood pressure, Ca homeostasis, and enzyme activities [14]. In specific, Na is the component of biological apatite $(Ca,Na,Mg)_{10}(PO_4,HPO_4,CO_3)_6(OH,F,Cl)_2$ [15]. Despite the high reactivity alkali elements have, previous studies have shown that Mg-based second

* Corresponding authors.
E-mail addresses: qin@ort.cuhk.edu.hk (L. Qin), yfzheng@pku.edu.cn (Y. Zheng).
[1] These authors contributed equally to this work.

https://doi.org/10.1016/j.cej.2020.127616
Received 23 July 2020; Received in revised form 5 October 2020; Accepted 29 October 2020
Available online 4 November 2020

phases with alkaline earth metal element Ca can work as anodes during the corrosion of biodegradable Mg alloys to protect matrix, and the refinement and well-distribution of the second phase can significantly lower the corrosion rate of the alloy [16]. However, to incorporate alkali elements into biodegradable Mg alloys faces challenges; the difficulties lie in that (1) these elements (Na and K) do not form second phases with Mg, which makes its sole existence detrimental to the corrosion resistance due to galvanic corrosion, and (2) their boiling points are much lower which may cause extra thermal ablation.

Micro-alloying is the concept commonly used in steel, where the addition of the alloyed element (i.e. vanadium, niobium and/or titanium) is very limited but leads to significant improvement of strength and toughness [17]. Micro-alloying is an emerging concept in biodegradable zinc alloy development as well. Recent studies reported that the micro-alloyed Zn-Mg, Zn-Mn and Zn-Li experienced significantly increased mechanical properties [18–21]. In addition, micro-alloying makes it possible to incorporate Na into biodegradable magnesium alloys. Na and Sn (Tin) can form master alloy, by which means Na can be incorporated to biodegradable Mg alloys [22]. In addition, Sn is a well-recognized alloying element for biodegradable Mg alloys [23]. The addition of Sn can refine grain size and improve the mechanical properties with appropriate addition amount [23–26]. Sn is involved in the synthesis of thymosin, and may improve the synthesis of protein and nucleic acid, and the organics of Sn may exert antitumor effects [27]. Zn (Zinc) can enhance the mechanical properties and corrosion resistance while maintaining benign biocompatibility [28]. Furthermore, Zn can stimulate bone formation and mineralization by directly activating aminoacyl-tRNA synthetase in osteoblastic cells and stimulating cellular protein synthesis [29].

In the present study, in order to increase the mechanical property and corrosion resistance with essential element Na, by using Sn-Na master alloy, Na was micro-alloyed to fabricate MgSnZnNa alloy, and for the first time to investigate its potential as biodegradable Mg scaffold, with comparison to high purity Mg and Na-free MgSnZn alloy both *in vitro* and *in vivo*. Their mechanical properties, corrosion resistance, cell viability and ability for calvarial defect regeneration have been compared.

2. Materials and methods

2.1. Material microstructure and mechanical properties

As-cast Mg4.6Sn2.4Zn0.07Na and as-extruded Mg6Sn5Zn0.3Na alloys were evaluated. Details on the fabrication and treatment of Mg6Sn5Zn0.3Na alloy can be found in our previous work [30]. Samples extruded at 723 K was the focus of the current study. Mg6Sn5Zn alloy with the same treatment as well as high purity Mg worked as control. High-angle annular dark-field scanning transmission electron microscope (HAADF-STEM) using JEOL 2100F instrument (JEOL Ltd., Japan) coupled with energy dispersive spectroscopy (EDS) was employed at 200 kV. Samples for STEM were mechanically ground followed by ion milling to electron transparency with Gatan precision ion polishing system (PIPS). Samples with a diameter of 5 mm and a thickness of 2 mm were used for *in vitro* corrosion tests, and with a diameter of 5 mm and a thickness of 0.3 mm were adopted for *in vivo* model. X-ray diffractometer (XRD DMAX 2400, Rigaku) with Cu Kα radiation was used with a scan rate of 4°/min. Microhardness test was conducted via HVM-1000 tester (Shimadzu Corp., Japan). Data points were collected from 3 samples and for each sample, 3 random positions were selected for the testing.

2.2. In vitro biodegradation

Bulk pure Mg, Mg6Sn5Zn and Mg6Sn5Zn0.3Na alloy samples were cut and polished for electrochemical tests and immersion test. A three-electrode cell with a platinum plate as the counter-electrode and a saturated calomel electrode (SCE) as reference electrode was utilized for electrochemical evaluation in Hank's solution at room temperature. The electrochemical test was conducted to obtain Open Circuit Potential (OCP), corrosion potential (E_{corr}), corrosion current density (I_{corr}) and corrosion rate. The immersion test was conducted in Hank's solution at 37 °C with a solution volume/surface area ratio (V/S) of 20 ml·cm^{-2}. The pH change of the soaking solution was recorded daily for 20 d. For each experiment, 3 to 4 replicates were tested. After 3 d and 20 d immersion test, the corroded surface was rinsed with deionized water and dried for Scanning Electron Microscope (Hitachi S-4800 Emission Scanning Electron Microscopy, Japan) coupled with EDX.

2.3. Cell viability, morphology and PCR

MC3T3-E1 cells were used for cell viability test. In brief, cells were cultured in Dulbecco's Modified Eagle Media (DMEM) supplemented with 10% Fetal Bovine Serum (FBS), 100 U·ml^{-1} penicillin and 100 g·ml^{-1} streptomycin in a humidified atmosphere with 5% CO_2 at 37 °C. Sterilized samples were incubated in the culture media for 1 day at an extraction ratio of 1 cm^2·ml^{-1} to prepare extracts. 1 day after seeding of cells in 96 well plate at a density of 5×10^3 cells per 100 μL media, the culture media was replaced by extracts. At 1, 3 and 5 days before testing, the extracts were replaced by the cell culture medium to avoid interference [31]. Cell Counting Kit-8 (CCK-8, Dojindo Molecular Technologies, Japan) was utilized for cell viability. Cell morphology after 1 d culture in extract was observed via Confocal Microscope (A1R-si, Nikon) by staining FITC-phalloidin dye for microfilament and DAPI for nuclei. Mouse Adipose Derived Mesenchymal Stem Cells (ADSC, Cyagen) were adopted to test the osteogenesis *in vitro*. The cells, received in frozen form, were thawed, plated and expanded until passage 3. DMEM with addition of 10% FBS and antibiotics was prepared as growth media, whilst osteogenic media was purchased from Cyagen (Cat. No. GUXMX-90021), which composes of basal medium, FBS, Penicillin-Streptomycin, Glutamine, Ascorbate, β-Glycerophosphate and Dexamethasone. Passage 3 cells were seeded into 24 well plate at an initial seeding density of 3×10^3 cells per 100 μL media. To test the effects of Mg-Na co-release, $MgCl_2$ and NaCl were used to evaluate the impact on osteogenesis. 1 mM $MgCl_2$ or 1 mM $MgCl_2$ plus 3.6 μM NaCl (based on the weight ratio calculation from Mg6Sn5Zn0.3Na alloy) were added to growth media and osteogenic media every three days when replacing the media. At 7 and 14 days after cell culture, RNA were collected by using Trizol reagent under the protocol from the manufacture. Pure RNA was then converted to cDNA via iscript cDNA synthesis kit (Bio-Rad), and the cDNA was mixed properly with primers and universal sybr green master mix (Bio-Rad) and ran through an RT-qPCR machine (ABsystem). 4 primers including Collagen 1, Runx-2, Osteocalcin (OCN) and Osterix were tested with beta-actin working as housekeeping gene. The data was calculated by $2^{-\Delta\Delta Ct}$ method. Gene sequence can be found in Table 4.

2.4. Animal model and surgery

Totally 45 male Sprague Dawley Rats at the age of 4 months were utilized to evaluate the *in vivo* regeneration of the calvarial defect model. The *in vivo* model was approved by the Animal Experimentation Ethics Committee (AEEC) of the Chinese University of Hong Kong (15-207MIS-5C) and the surgery was conducted following a published protocol [32]. A 5 mm in diameter hole was created. Sterilized Mg alloys (Mg6Sn5Zn and Mg6Sn5Zn0.3Na) with 5 mm in diameter and 0.3 mm in thickness were implanted as scaffolds. The group with surgery but without implantation defines the Blank group. Several holes with a diameter of 600 μm were punched on the scaffolds to allow better blood circulation. 6 weeks and 12 weeks post-surgery, rats (n = 6 for each group at each time point) were executed for micro-CT, histological and immunohistochemistry evaluations. In another experiment, to test the relationship between angiogenesis and osteogenesis, 9 rats were randomly assigned to three groups, including blank repair group, Mg6Sn5Zn0.3Na implanted group + drug vehicle (saline containing 0.1% DMSO), and

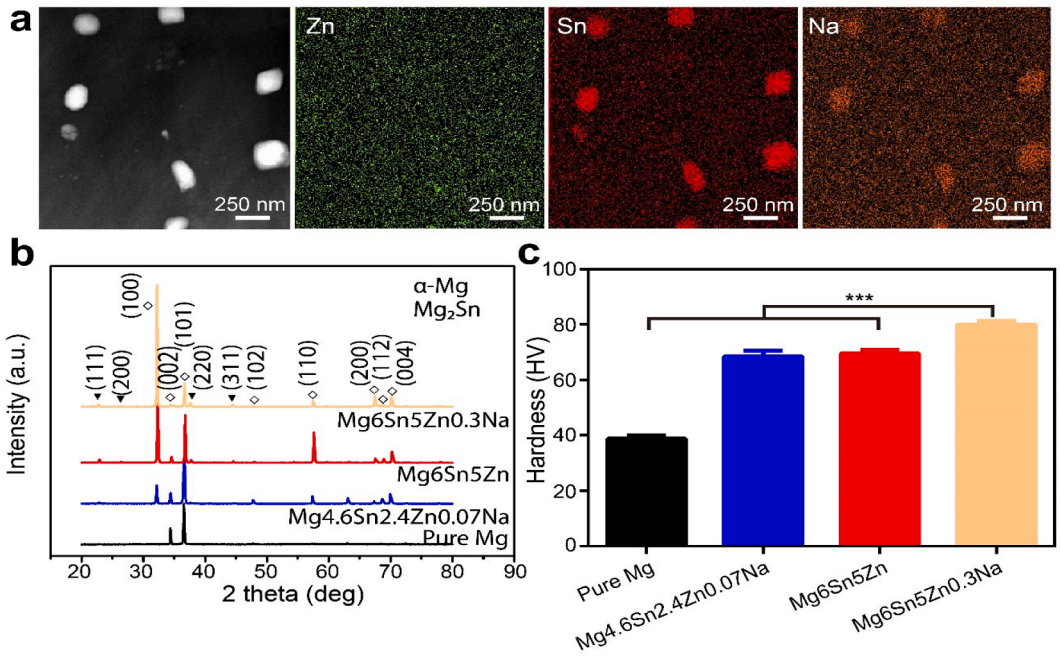

Fig. 1. Alloy microstructure, composition and mechanical properties. a HAADF-STEM image and corresponding EDS maps of Mg6Sn5Zn0.3Na. Na is uniformly distributed in the Sn-containing second phase (Mg_2Sn). It does not just coat the second phase surface but also inside the spherical second phase. b Phase composition acquired via X-ray diffraction (XRD). b Microhardness comparison of the alloys. The data (n = 9) were expressed as mean ± standard deviation (SD). ***: $p < 0.001$.

Mg6Sn5Zn0.3Na + VEGFR-2 inhibitor SU5416 group (n = 3 rats per group). SU5416 (Cat. No.: HY-10374, 100 μM, 0.1 ml/48 h) was subcutaneously injected (above the calvarial defect region). At week 3, the rats from all groups were perfused with micro-fil (a contrast) before sacrificed. After processed to micro-CT angiography immediately (no bone islands could be detected at this time point according to our pilot study), the fresh samples were homogenized with protein extraction buffer (RIPA), to analyze the osteogenic markers with western blotting.

2.5. Micro-Computed Tomography (Micro-CT) and angiography

Samples were wrapped in wet gauze and fitted in the sample tube before micro-CT scanning (μCT40, Scanco Medical, Brüttisellen, Switzerland). The samples were scanned under 70 kVp, 114 μA, and 190 ms of integration time, with resolution set at 15 μm per voxel and 1024 × 1024 pixels. The region of interest (ROI) was selected from 2D images with set thresholds (>180) as mineralized tissue, according to the tuning. 3D reconstruction of the mineralized tissue was performed. A low-pass Gaussian filter (Sigma = 0.8, Support = 1.0) was used for 3D reconstruction. Quantitative analysis involved all slides of the 2D images. Morphometric parameters included total volume (TV), bone volume (BV), and BV/TV were analyzed. For angiography, the vessels were mapped with threshold set at >180.

2.6. Fluorescence labelling, histological and immunohistochemistry (IHC)

Sequential fluorescent labelling was adopted to evaluate new bone formation. At 4 weeks and 10 weeks post-surgery, Calcein green (CG, 5 mg/kg, Sigma-Aldrich, USA) was injected subcutaneously. At 5 weeks and 11 weeks post-surgery, Xylenol Orange (XO, 90 mg/kg, Sigma-Aldrich, USA) was injected in the same way. At 6 weeks and 12 weeks post-surgery, rats were executed, and regions of interest (ROI) were embedded in methyl methacrylate (MMA). A fluorescence microscope (Leica Q500MC, Leica, Germany) was utilized for observation. As for histological and IHC, samples were decalcified and embedded in paraffin. Hematoxylin and Eosin (*H&E*) staining were adopted for histological, Calcitonin gene related peptide (CGRP), Osteocalcin (OCN) and basic fibroblast growth factor (bFGF) and Vascular Endothelial Growth Factor (VEGF) antibody (Abcam, UK) were selected for IHC.

2.7. Regenerative tissue hardness and element distributions

12 weeks post-surgery, sample slices were collected and measured for microhardness (SHIMADZU Dynamic Ultra-micro Hardness Tester DUH-211/DUH-211S, Japan) at a load of 245 mN with 10 s loading time and 5 s unloading time. Both the defect interface and non-defect interface were tested. 5 replicates were measured. To verify the element distribution in regenerative tissue 12 weeks post-surgery, unstained sections were polished, rinsed in deionized water and dried in air. Afterwards, sample images were captured with SEM couple with EDS. Three replicates are utilized.

2.8. Statistical analysis

One-way analysis of variance (ANOVA) followed by Tukey's *post hoc* test was used. A p-value < 0.05, p-value < 0.01, p-value < 0.001, respectively was considered statistically significant.

3. Results

3.1. Characterization of biodegradable MgSnZnNa alloys

High-angle annular dark-field scanning transmission electron microscopy (HAADF-STEM, Fig. 1a) showed element distribution in the Mg6Sn5Zn0.3Na alloy used in the current study. Na was evenly distributed throughout the Sn-containing secondary phase, with no preference for partitioning to particle/matrix interface. This indicated that Na was not only deposited on the surface but also diffused into the particles, because of the post treatment. Zn remained mostly in solid solution in the a-Mg matrix. For alloy composition, no peaks of Zn-containing phase were found on XRD (Fig. 1b) after the addition of Sn, Zn and Na, compared with high purity Mg. Higher concentration of Sn and Zn resulted in the higher intensity of Mg_2Sn. Besides, according to Fig. 1a and Fig. 1b, it could be concluded that all the alloys added with

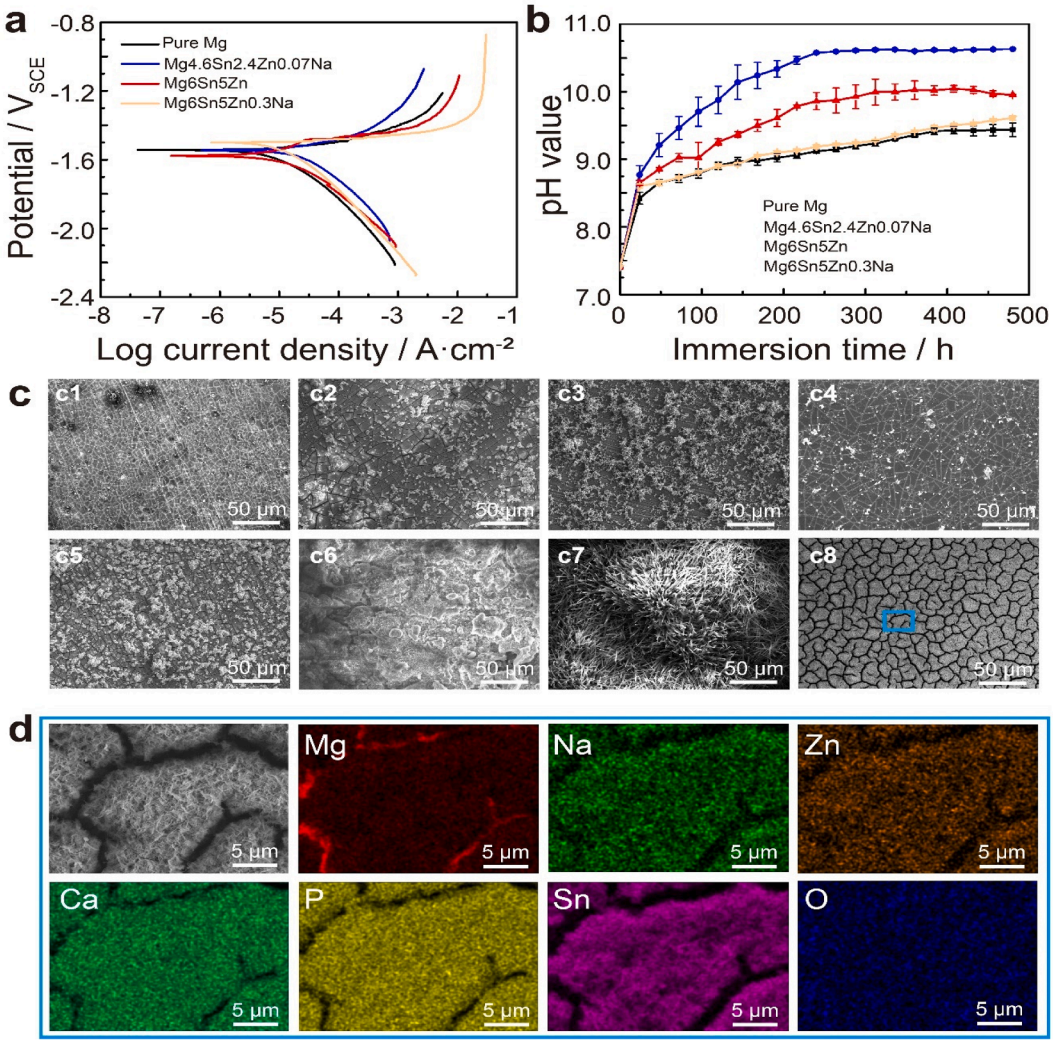

Fig. 2. *In vitro* biodegradation test. a potentiodynamic polarization test. b pH value monitoring during immersion in Hank's solution. Mg6Sn5Zn0.3Na presented similar trend to high purity Mg, which is significantly lower than Mg4.6Sn2.4Zn0.07Na or Mg6Sn5Zn. c surface corrosion products morphologies after 3d (c1-c4) and 20 d (c5-c8) immersion. c1 and c5 pure Mg, c2 and c6. Mg4.6Sn2.4Zn0.07Na, c3 and c7 Mg6Sn5Zn, c4 and c8 Mg6Sn5Zn0.3Na. d EDS mapping of Mg, Na, Zn, Ca, P, Sn and O distribution of the labelled zone in c8. Mg6Sn5Zn0.3Na after 20 days immersion presented even corrosion products formation which contained large amount of Ca, P, as well as Na, Sn and Zn.

Table 1
Open circuit potential, corrosion potential (E_{corr}), corrosion current density (I_{corr}) and corrosion rate values obtained from the electrochemical tests.

	OCP (V_{SCE})	E_{corr} (V_{SCE})	I_{corr} ($\mu A \cdot cm^{-2}$)	Corrosion rate ($mm \cdot y^{-1}$)
Pure Mg	$-(1.62 \pm 0.03)$	$-(1.55 \pm 0.01)$	7.8 ± 0.5	0.18 ± 0.01
Mg-4.6Sn-2.4Zn-0.07Na	$-(1.57 \pm 0.01)$	$-(1.54 \pm 0.01)$	16 ± 1	0.35 ± 0.03
Mg-6Sn-5Zn	$-(1.59 \pm 0.02)$	$-(1.57 \pm 0.03)$	14 ± 1	0.32 ± 0.01
Mg-6Sn-5Zn-0.3Na	$-(1.56 \pm 0.01)$	$-(1.50 \pm 0.01)$	9 ± 3	0.19 ± 0.07

Zn remained mostly in solid solution in the α-Mg matrix. Since no Mg-Zn based second phase formed and no solid solubility of Na in Mg was observed, Na partitioned only to the Mg-Sn secondary phase. Moreover, Mg6Sn5Zn0.3Na resulted in 106%, 17% and 15% higher hardness than pure Mg, Mg4.6Sn2.4Zn0.07Na and Mg6Sn5Zn counterpart (Fig. 1c), respectively, due to the diffusion of micro-alloyed Na into Mg_2Sn phase.

3.2. *In vitro* biodegradation

The *in vitro* biodegradation properties were determined by electrochemical test and immersion test. Fig. 2a presented the potentiodynamic polarization curve, with the calculated OCP, E_{corr}, I_{corr} and corrosion rate presented as Table 1. The combined addition of Sn, Zn and Na altered the OCP and E_{corr}. However, the addition of Na did not lower the OCP and E_{corr}, as compared with Mg6Sn5Zn. This could be ascribed to the fact that Na presented a uniform distribution in second phase, which reduced the negative effects on corrosion potential. In addition, micro-alloyed Na along with its distribution after the post-treatment helped to decrease the corrosion potential difference between the α-Mg matrix and second phase, resulting in a doubled corrosion resistance compared to Mg6Sn5Zn, due to a reduced galvanic effect between the matrix and the second phase. Actually, the even distribution of Na in Mg_2Sn is critical to the corrosion resistance. It's known that the galvanic effect between matrix and second phase in Mg alloy corrosion weakens the corrosion resistance of Mg alloys, regardless of who plays the role of cathode [33]. The idea to use rare earth elements in Mg alloys is considered to reduce the corrosion potential difference between the matrix and second phase as well as purify the alloy matrix and therefore reduce the galvanic effect [34,35]. If Na deposition on Mg_2Sn only formed a shell, it would

Table 2
EDS results (at.%) of the corrosion products after 3 days immersion in Hank's solution.

	C	O	Na	Ca	Mg	P	Zn	Sn
Pure Mg	4.88	66.97	\	13.70	6.45	8.00	\	\
Mg-4.6Sn-2.4Zn-0.07Na	5.84	72.69	0.11	1.57	17.46	1.82	0.32	0.18
Mg-6Sn-5Zn	3.24	55.06	\	11.02	21.78	7.13	0.86	0.52
Mg-6Sn-5Zn-0.3Na	3.04	59.15	1.02	16.16	11.39	8.85	0.01	0.39

Table 3
EDS results (at.%) of the corrosion products after 20 days immersion in Hank's solution.

	C	O	Na	Ca	Mg	P	Zn	Sn
Pure Mg	4.44	71.70	\	11.64	4.22	8.00	\	\
Mg-4.6Sn-2.4Zn-0.07Na	\	68.39	\	0.02	30.54	0.21	0.68	0.16
Mg-6Sn-5Zn	2.87	73.96	\	\	17.11	\	\	\
Mg-6Sn-5Zn-0.3Na	4.73	62.52	0.56	15.01	6.33	10.41	\	0.43

Table 4
Gene sequence for RT-qPCR.

	Forward (5′-3′)	Reverse (5′-3′)
β-actin	TCC TCC TGA GCG CAA GTA CTC T	CGG ACT CAT CGT ACT CGT GCT T
Collagen 1	CCA AGA AGA CAT CCC TGA AG	GTG CCA TTG TGG CAG ATA
Runx-2	AAT GCC TCC GCT GTT ATG	GGG AGG ATT TGT GAA GAC TG
Osteocalcin	CAA GCA GGA GGG CAA TAA G	CGT CAC AAG CAG GGT TAA G
Osterix	GGA AAG GAG GCA CAA AGA A	GTC CAT TGG TGC TTG AGA A

introduce a third electrode in the galvanic effect, and probably the corrosion resistance will not be as good as the current form.

Fig. 2b revealed the pH change of the Hank's solution during *in vitro* degradation of the alloys. Significant difference occurred 72 h after immersion, when the pH change rates (curve slope) of Mg6Sn5Zn0.3Na and high purity Mg were comparable but those of Mg6Sn5Zn and Mg4.6Sn2.4Zn0.07Na were much higher. The pH value of Mg4.6Sn2.4Zn0.07Na and Mg6Sn5Zn stabilized at ~10.5 and ~10 after 10 d and 13 d immersion, respectively. In the meantime, high purity Mg and Mg6Sn5Zn0.3Na reached their highest pH value of ~9.5 at day 20. Fig. 2c and Fig. 2d presented the surface corrosion products aggregation, with the detailed EDS elemental composition shown in Table 2 and Table 3. High purity Mg showed a typical morphology of pitting after 3 d immersion, with C, O, Ca, Mg and P detected via EDS. As for Mg4.6Sn2.4Zn0.07Na and Mg6Sn5Zn, non-uniform corrosion morphology with corrosion products as well as cracking emerged especially after 20 d immersion. In comparison, less corrosion products were found on the surface of Mg6Sn5Zn0.3Na after 3 d immersion, while after 20 d immersion quite uniform corrosion products formed. The corresponding elemental distribution implied large number of Ca and P deposition on the surface as well as corrosion products related to the alloy elements Mg, Na, Zn and Sn. Among all the alloys, Mg6Sn5Zn0.3Na has the most Ca-P deposition (Table 2 and Table 3). This was in good accordance with previous bioceramic studies in which the apatite layer increased following the addition of Na_2O and P_2O_5 both *in vitro* and *in vivo* [36,37].

3.3. In vitro biocompatibility and osteogenesis

The cell morphologies were shown in Fig. 3a. MC3T3-E1 cells performed benign response to the extracts of all the alloys with good spreading shape. The extract viability was shown in Fig. 3b. In details, the extracts of Mg6Sn5Zn and Mg6Sn5Zn0.3Na showed decrease to $86 \pm 3\%$ and $83 \pm 6\%$ respectively on the viability at Day 1, which was recovered and showed no significant difference with high purity Mg after 5 days ($P > 0.01$). In addition, to test the specific osteogenic effects of Mg^{2+} and Na^+, Mg^{2+} and Na^+ were supplemented for both growth medium and osteogenic medium. With 1 mM Mg^{2+} addition, significant higher expressions of OCN and Osterix were found after 14 d culture in growth media. In comparison, the combined addition of 1 mM Mg^{2+} and 3.6 μM Na^+ was found to upregulate the expression of OCN and Osterix after 7 d culture in growth medium and upregulate the expression of OCN in osteogenic media after 14 d differentiation. Moreover, the combined addition of Mg and Na seemed to advance the upregulated expression of OCN and Osterix in growth media (Fig. 3c), which might accelerate the bone regeneration *in vivo*.

3.4. Rat calvarial defect regeneration

To investigate the effects of Na-incorporated Mg scaffold on bone regeneration *in vivo*, calvarial defect model was employed according to previous protocol in rat (Fig. 4). A 5 mm defect was created with small holes punched to make the mesh-implant to allow blood vessel ingrowth (Fig. 4a-f). Micro-CT imaging along with derived bone volume density (BV/TV) after 6 and 12 weeks were presented in Fig. 5a-b. No significant bone mineralization ($8.82 \pm 1.09\%$ at week 6 and $7.91 \pm 1.58\%$ at week 12) was found in the blank/sham group over time, while MgSnZn scaffold showed limited bone mineralization after 6 weeks ($18.38 \pm 2.03\%$) and 12 weeks ($21.41 \pm 2.55\%$). In comparison, Na-incorporated Mg scaffold showed a significant higher bone mineralization in the defects which accounted for $37.17 \pm 4.13\%$ after 6 weeks and $42.84 \pm 3.92\%$ after 12 weeks. In consistence, pixel-based bone coverage of the defect showed that the new bone coverage for MgSnZnNa is 88.48% after 12 weeks implantation, which was much higher than the MgSnZn (43.02%) or blank (7.49%). Besides, most new bone was found formed at the edge of the defects in Mg6Sn5Zn group. According to the scoring system described in the protocol [32], bony bridging over partial length of defect (scoring 3) and bony bridging entire span of defect at longest point (diameter) (Scoring 4) were found in Na-incorporated Mg scaffold 6 weeks and 12 weeks after implantation, respectively. In contrary, no bony bridging over length was found in the blank or Mg scaffold groups. The scoring for different group after 6 weeks and 12 weeks was shown in Fig. 5c.

The fluorescent labelling of CG and XO was presented in Fig. 6a. Significant fluorescent labeling of CG and XO were found in both Mg6Sn5Zn and Mg6Sn5Zn0.3Na 6 weeks post-surgery, while very limited labeling was found in sham group, indicating the Mg-based materials in the present study both improved new bone formation. Furthermore, by comparing Mg6Sn5Zn and Mg6Sn5Zn0.3Na, a significantly thicker and more uniformed new bone bridge could be found in Mg6Sn5Zn0.3Na group, while the new bone thickness varied in the defect area of Mg6Sn5Zn. At week 12 post-surgery, the new bone thickness in Mg6Sn5Zn0.3Na group continuously increased compared with week 6 results. The new bone bridge has formed in the defect area with a uniform thickness which was similar to the surrounding old bone. In comparison, neither the blank group nor Mg6Sn5Zn group showed continuously increased new bone formation between 6 weeks post-surgery and 12 weeks post-surgery. The sequential fluorescent labeling results were in good accordance with our previous micro-CT results.

Fig. 6b presented the *H&E* image of the calvarial defect area 6 weeks and 12 weeks post-surgery. New bone formed gradually from the periphery old bone to the middle, from top to bottom for both Mg6Sn5Zn and Mg6Sn5Zn0.3Na groups. The blank group barely showed new bone

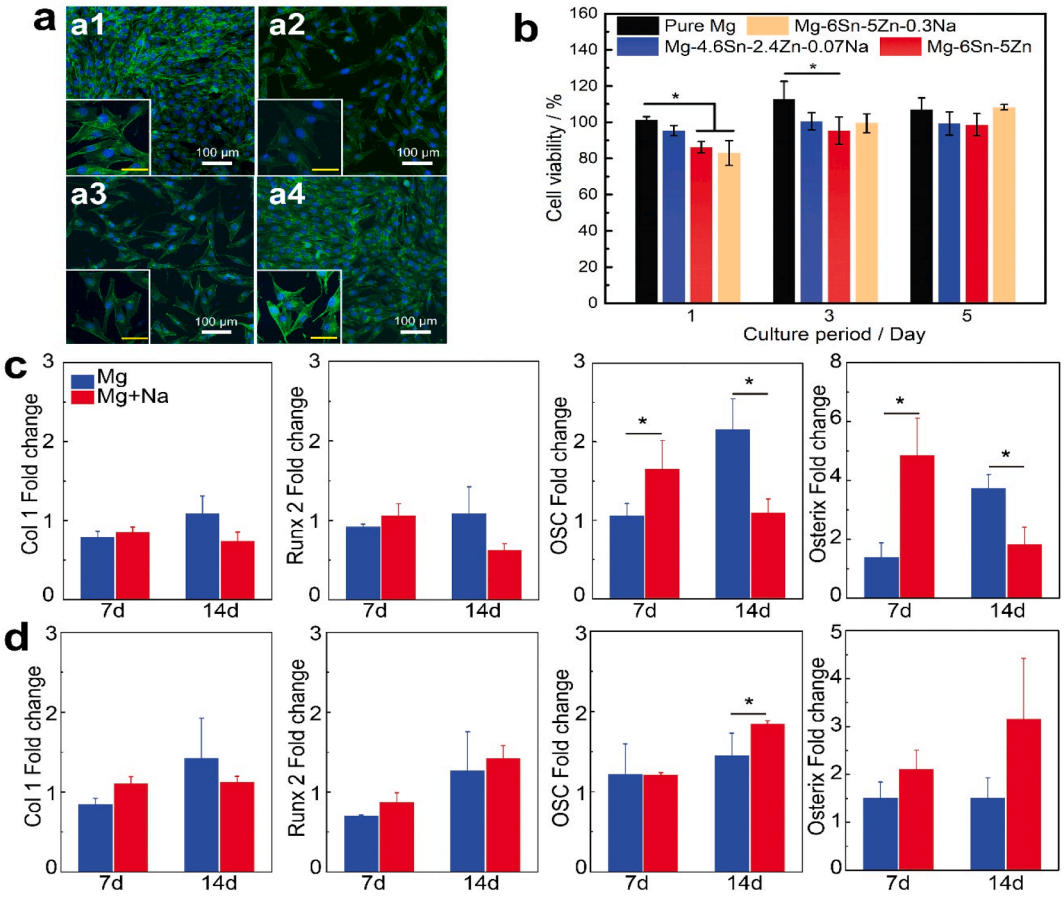

Fig. 3. *In vitro* viability and osteogenesis. a MC3T3-E1 cell morphology presented by FITC-DAPI after cultured in the extract of (in sequence from a1 to a4) pure Mg, Mg4.6Sn2.4Zn0.07Na, Mg6Sn5Zn and Mg6Sn5Zn0.3Na. b Viability of MC3T3-E1 cultured in the alloy extracts. The data (n = 5) were expressed as mean ± standard deviation (SD). c Gene expression of mouse ADSCs cultured in growth media with extra Mg and Na addition. d Gene expression of mouse ADSCs cultured in osteogenic media with extra Mg and Na addition. The data (n = 3) were expressed as mean ± standard deviation (SD). *: $p < 0.05$ and **: $p < 0.01$.

formation 6 weeks and 12 weeks post-surgery. As for Mg6Sn5Zn and Mg6Sn5Zn0.3Na groups, new bone performed a compact contact to the surrounding old bone, and more new bone formed on the bottom of the defect area 12 weeks post-surgery. In comparison, in Mg6Sn5Zn0.3Na group, not only thicker new bone was observed but also higher reactivity of new bone osteoblast was found in the defect area, indicating enhanced regeneration.

To compare the mechanical properties, microhardness test was conducted with the results plotted in Fig. 6c. The microhardness of the non-defect interface in blank group was HV 63 ± 5, while those in Mg6Sn5Zn and Mg6Sn5Zn0.3Na groups were HV 73 ± 2 and HV 77 ± 5, respectively, indicating that the non-defect interface showed a higher hardness after the implantation of Mg alloys ($p < 0.001$). As for defect interface, the microhardness of blank, Mg6Sn5Zn and Mg6Sn5Zn0.3Na are HV 19 ± 2, HV 23 ± 3 and HV 36 ± 4, respectively. Mg6Sn5Zn0.3Na group presented the highest microhardness compared with blank group ($p < 0.001$) and Mg6Sn5Zn group ($p < 0.01$).

Fig. 7 presented the IHC staining of CGRP, OCN, bFGF and VEGF at 6 weeks post-surgery. The results suggested the increased expression of CGRP in both Mg6Sn5Zn and Mg6Sn5Zn0.3Na groups, and the Mg6Sn5Zn0.3Na group showed the highest expression. This was in good accordance with previous study in which Mg induced osteogenesis via increased CGRP expression [3]. Besides, we also found that the Mg6Sn5Zn and Mg6Sn5Zn0.3Na implants could enhance the expression of OCN *in vivo*, especially after the implantation of Mg6Sn5Zn0.3Na sample. Previous study has demonstrated that magnesium phosphate minerals improved the expression of OCN when culturing MC3T3-E1 *in vitro* [38]. Meanwhile, the higher expression of OCN in Mg6Sn5Zn0.3Na group was in good accordance with our *in vitro* PCR results (Fig. 3b,c). Moreover, our results showed that dramatically higher expression of VEGF, an angiogenic marker critical for bone formation [39], in Mg6Sn5Zn0.3Na group than Mg6Sn5Zn and blank groups.

At week 3, angiography showed that Mg6Sn5Zn0.3Na group distributed with more dense vessels in the defect region, accompanying with significantly higher expression of OCN and Osterix, as compared to blank repair group (Fig. 8a-b). SU5416 dramatically blocked the promotive effects of this Mg alloy on angiogenesis and osteogenesis (Fig. 8a-b). OCN and Osterix were significantly lower in the Mg-alloy implanted + SU5416 treated group as compared to the group received only Mg alloy implantation, further suggesting that angiogenesis plays an indispensable role in the Mg-alloy-enhanced bone regeneration. Fig. 9 presented the microstructure as well as elemental distribution in the defect 12 weeks after the implantation of Mg6Sn5Zn0.3Na. A large fraction of new bone formation was observed with no evidence of scaffold residue. The zoom-in image showed the microstructure of new bone formed inside the defect. Blood capillary-like structures (in accordance with VEGF staining) were observed inside new bone, indicating the proper function of new bone formed. C, P, Mg, Na and limited Sn and Zn were found in the new bone. Interestingly, the composition of Mg and Na along NB (new bone inside the defect)-Non (non-bone area inside the defect)-OB (old bone outside the defect) direction followed the same trend, in which is the most was found in NB and the least in Non group. This was clearer for Na distribution, where its content in NB is significantly higher than that in OB ($p < 0.01$) or Non ($p < 0.001$). It's known that both elements Mg and Na are the components of biological apatite/healthy bone [14]. The element distribution results indicate that both Mg and Na

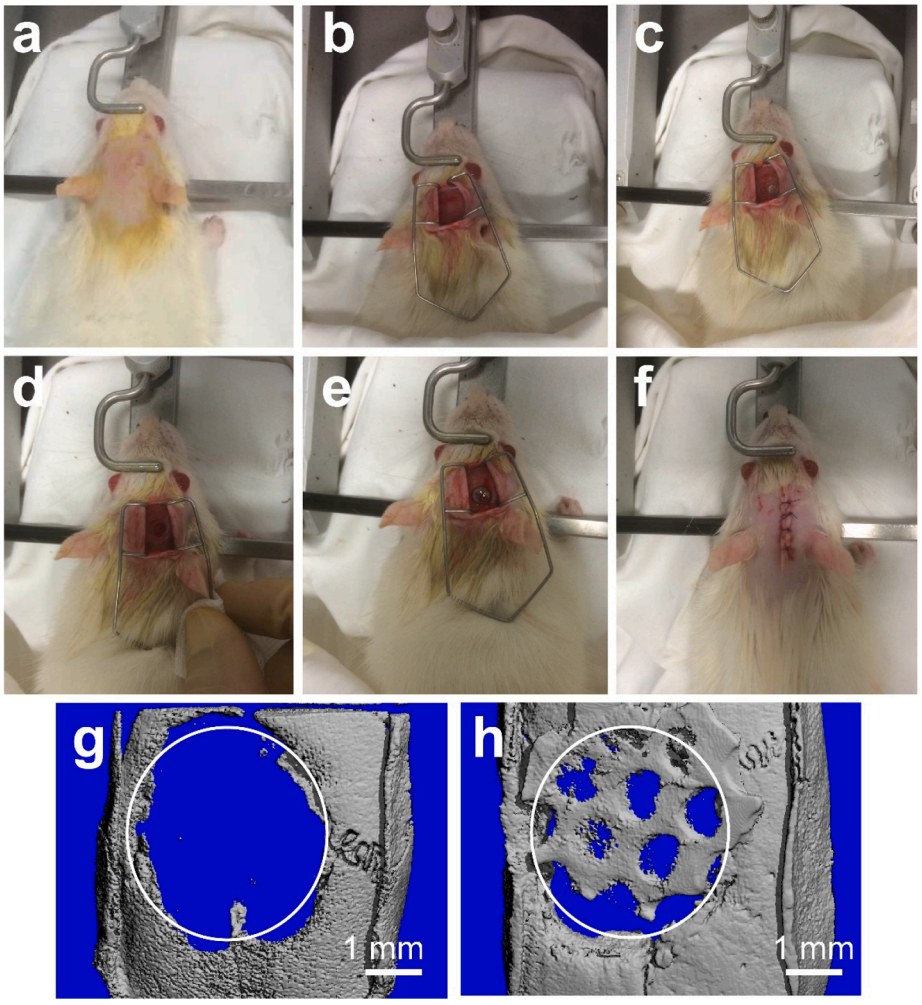

Fig. 4. Procedures for establishing the rat calvarial defect model (a-f). g Defect area without implantation. h defect area with MgSnZnNa scaffold implantation.

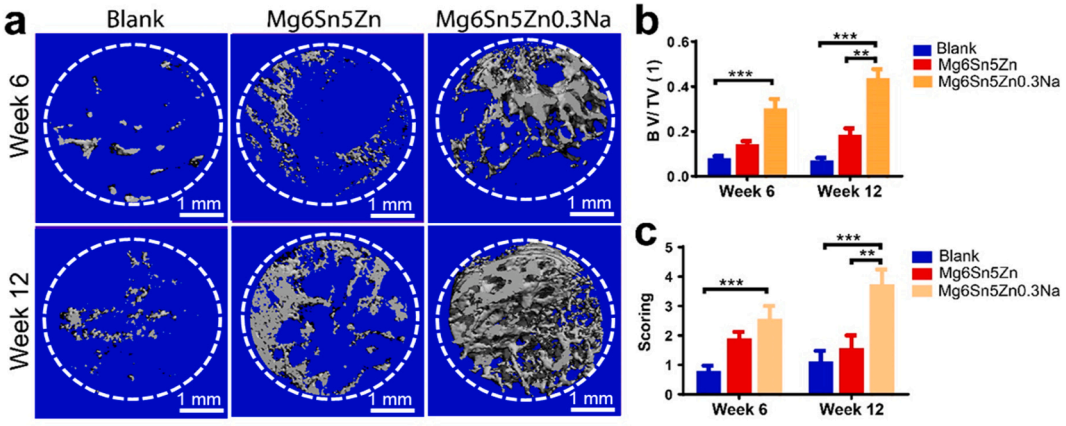

Fig. 5. *In vivo* micro-CT quantification of new bone formation. a 3D reconstruction of micro-CT images at 6 weeks and 12 weeks after implantation. b BV/TV calculated via micro-CT. c Scoring evaluation according to calvarial defect model protocol.[32] The data (n = 5 per group) were expressed as mean ± standard deviation (SD). **: $p < 0.01$ and ***: $p < 0.001$.

elements were involved in the new bone formation during calvarial defect regeneration, and the co-release of Mg and Na ions possibly accounted for the better regeneration as observed in Mg6Sn5Zn0.3Na group.

4. Discussion

In summary, we demonstrate for the first time a Na micro-alloyed biodegradable Mg-based scaffold that achieves a unique co-release of Mg and Na for enhancing bone regeneration. This is an aluminum and rare earth element -free alloy which has achieved increased hardness as

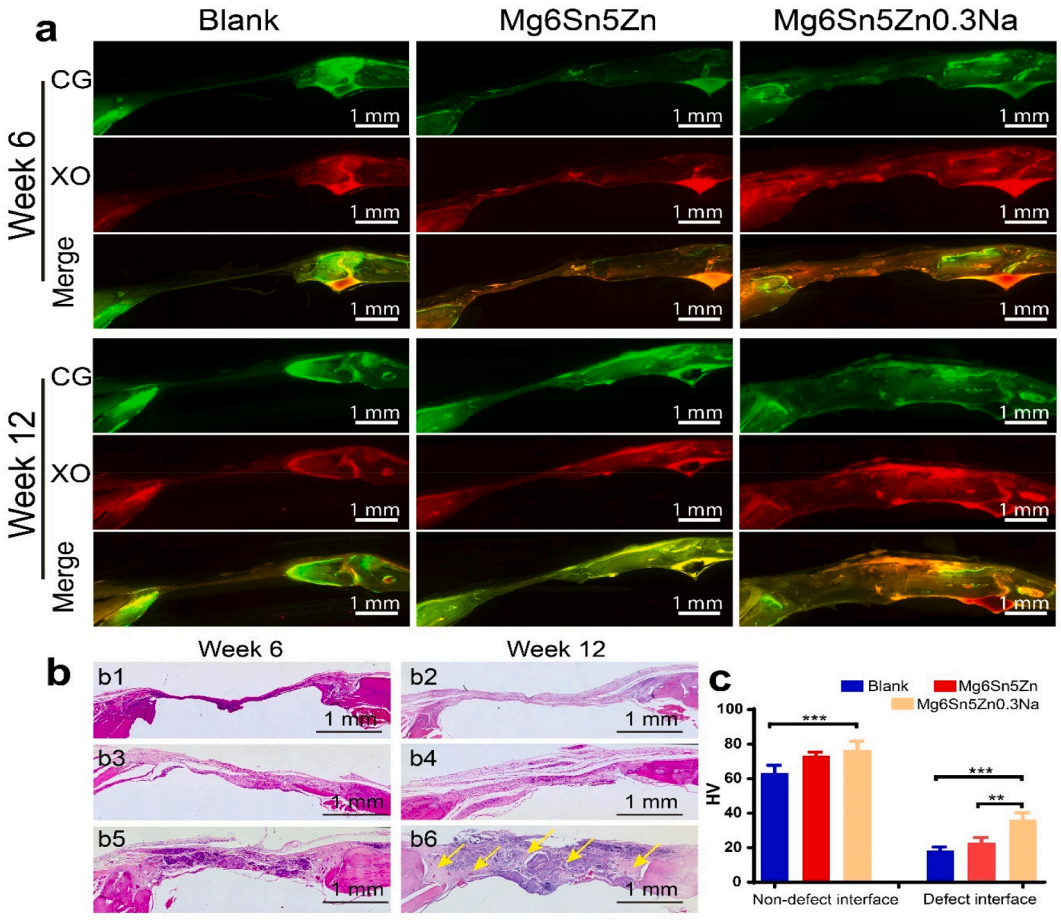

Fig. 6. Evaluation of new bone formation via fluorescent labeling, staining and hardness. a Calcein Green (CG) and Xylenol Orange (XO) sequential fluorescent labeling. b Haematoxylin and Eosin (*H&E*) staining. b1 and b2 for Blank group, b3 and b4 for Mg6Sn5Zn, and b5 and b6 for Mg6Sn5Zn0.3Na. Yellow arrows indicated the newly formed bone within the defect region. c Microhardness comparison in both non-defect interface and defect interface at 12 weeks post-surgery. The data (n = 5) were expressed as mean ± standard deviation (SD). **: $p < 0.01$ and ***: $p < 0.001$. (For interpretation of the references to colour in this figure legend, the reader is referred to the web version of this article.)

well as enhanced corrosion resistance at the same time without surface modification. The even diffusion of Na in Mg_2Sn and the solid soluble Zn in Mg contribute to reduce the galvanic effects of the alloys, with which a more homogeneous corrosion behavior is observed. Subsequently, we demonstrate *in vivo* enhanced bone regeneration in calvarial defect model in rats, compared with Na-free Mg alloy counterpart.

In practice, bioceramics, including hydroxyapatite (HA) and β-tricalcium phosphate (β-TCP), usually have good osteogenic effects due to the high content of calcium and phosphates. A comparison has been made to evaluate the osteogenic effects of the present work to recent calvarial defect regeneration work (Fig. 10a). The mineralized bone percentage is much higher compared with other Mg alloy or Mg-modified ceramic and polymer studies [40–48]. Compared with TCP, HA and cell coculture based materials, the current MgSnZnNa alloy scaffold also showed superior bone mineralization to most of the works reported [49–59].

Mg^{2+} is known to promote osteogenesis by upregulating the expression of CGRP [3], which is also observed in the current study. The unique property of Mg makes it good composition in orthopedic implants, either as matrix or doped functional ions [60–62]. Zinc is thought to act on the process of bone-resorbing factors-induced protein kinase C activation, which is involved in Ca^{2+} signaling in osteoclastic cells. Zinc plays a role in the preservation of bone mass [63]. More importantly, the present study demonstrates a Mg-Na co-release strategy for enhanced bone regeneration (Fig. 10b). The single effect of Na on osteogenesis has been rarely reported. In specific, a very recent study has also demonstrated sodium graphene phosphate (NaGP) increased the alkaline phosphate (ALP) expression of human Mesenchymal Stem Cells and osteogenic gene expression after 10 d and 14 d culture in growth media, respectively [64]. Besides, the microalloying of Na significantly promotes the expression of OCN and VEGF besides CGRP *in vivo*, and the addition of Na^+ upregulates and advanced the expression of OCN during mouse ADSC osteogenic differentiation *in vitro*. The addition of Na makes the alloy more favorable for bone regeneration by promoting osteogenesis and angiogenesis at the same time. A recent study has shown that angio-osteogenesis was the mechanism for an implanted MgCaZn alloy in femoral condyle of Sprague Dawley rats [65]. The current study, found angiogenesis aided osteogenesis for improved bone regeneration in a rat calvarial defect model, after the implantation of newly MgSnZnNa alloy. Despite the coupling effects of angiogenesis and osteogenesis found in both studies, the different alloy composition and different implantation site imply that angio-osteogenesis may be the common underlying mechanism underlying their bone regeneration effects after *in vivo* biodegradation. In the present study, the angio-osteogenesis may be due to the higher expression of CGRP [39]. In the meantime, the release of Na^+ can regulate the formation of biological apatite. It's known that the carbonate ion can substitute for both OH in the c-axis apatite (type A carbonate) and the phosphate group (type B carbonate) in HA. By evaluating various substituted HA, Na-bearing type A-B carbonate hydroxyapatite is considered similar both in chemical composition and infrared spectra to biological apatite, indicating Na is indispensable for biological apatite [66]. This is also confirmed by our

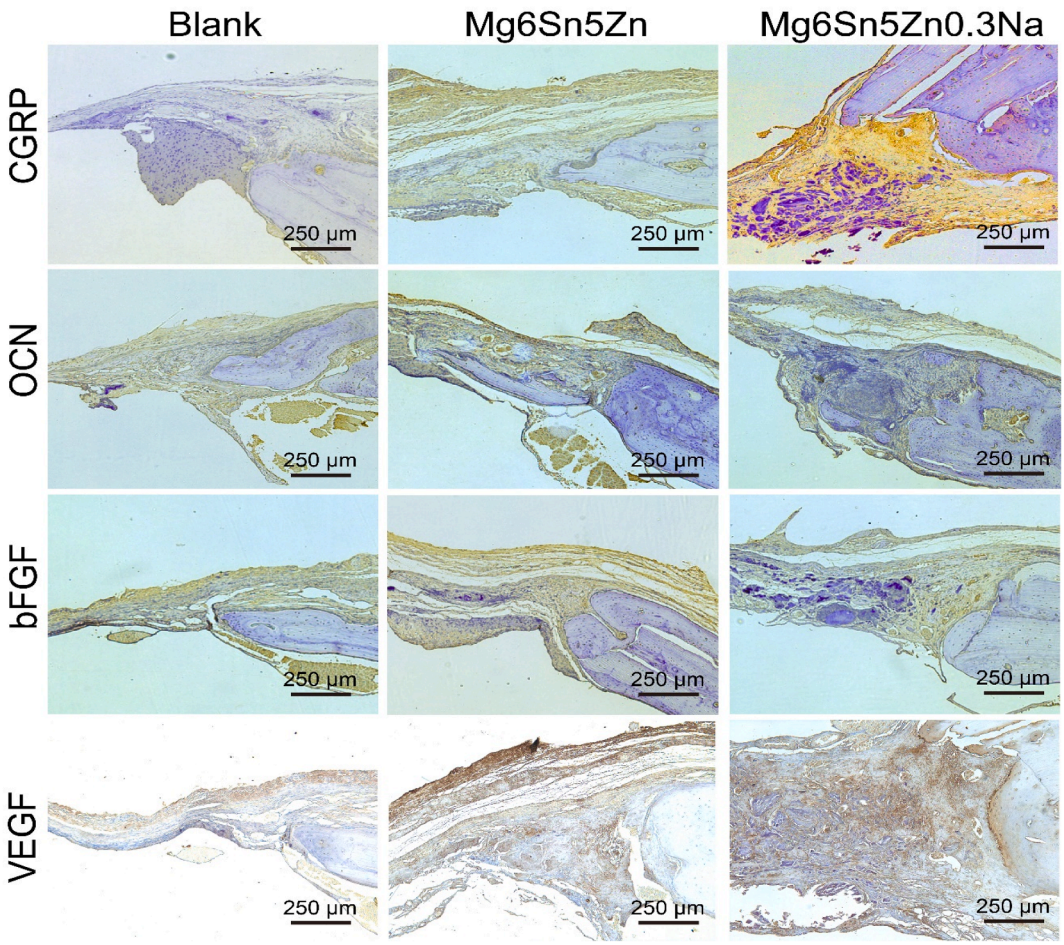

Fig. 7. IHC staining of CGRP, OCN, bFGF and VEGF at 6 weeks post-surgery.

EDS results for the old bone and new bone. Furthermore, biological apatite formation is considered a multi-step formation including ionic exchange with medium, amorphous matrix formation, nano-crystals formation, crystal fusion and crystal growth and c-axis orientation, in which Na plays significant role throughout [67]. At first, Na^+ quickly occupies some positions in the lattice, enhancing the substitution of PO_4^{3-} for CO_3^{2-} and promoting the release of Mg^{2+} [67]. Due to Na^+ substitution, the charge of HAp structure is destabilized, which facilitates the substitution of PO_4^{3-} by CO_3^{2-} to balance the total charge. In addition, the replacement of the phosphate group by a carbonate is charge compensated by the substitution of Na^+ for Ca^{2+} is energetically favorable ($\Delta H_{Na} = -71 kJ\ mol^{-1}$) [68]. In general, Na^+ regulates the formation of biological apatite by increasing the kinetic formation of apatite, facilitating the carbonation process and therefore enhancing osteoconductivity [67]. However, media extract study needs to be done in the future to see a full picture of the effects of alloy degradation to osteogenesis, as well as if there is any element synergism.

Furthermore, other factors may also be involved during the regeneration process. Previous study demonstrated low concentration supplement of Na^+ significantly increased the osteogenic transcription of Cbfa1 (Core-binding factor al), OPN and OCN, as well as epithelial sodium channel (ENaC) gene expression to promote osteogenesis of osteoblast [69]. Besides the co-release of Na^+ and Mg^{2+} on bone regeneration, the addition of Na in the current study altered the corrosion behavior and therefore the hydrogen evolution rate and the local pH value, which may also contribute. Researches have shown that hydrogen can selectively react with the hydroxyl radical (the most cytotoxic of reactive oxygen species) and therefore protect cells effectively [70]. It has been also reported that hydrogen can prevent neuronal apoptosis [71]. More importantly, hydrogen can affect the osteogenic differentiation of stem cells as well [72].

The Mg6Sn5Zn0.3Na alloy is promising not only because the degree of bone regeneration it achieved *in vivo* due to the co-release of Mg^{2+} and Na^+, but also it provided a new insight to utilize master alloy to micro-alloy essential elements (such as Na and K) or functional elements to biodegradable magnesium alloys. The composition of essential elements or biocompatible elements can eliminate the concern regarding the potential toxicity of other elements, while the function of the alloy get enhanced at the same time. However, the challenge remains such as to precisely control the addition of essential elements in the alloys during the multi-step casting procedure and post treatments, because of the high reactivity of these elements. Meanwhile, due to no solubility of Na in Mg, the single addition of Na may further enhance the corrosion rate since the two components are both with high reaction activity, as well as introduce brittleness. Moreover, being essential elements only means they are safer compared with other alloying elements. Nevertheless, it does not mean that the addition of these elements can be as much as desirable, as too high addition of essential elements can also cause body disorders, such as hypertension or hyperkalemia. Last but not the least, more detailed comparison between this newly fabricated alloy and other conventional or clinically proven biodegradable alloys need to be done for better understanding in the future.

Declaration of Competing Interest

The authors declare that they have no known competing financial interests or personal relationships that could have appeared to influence the work reported in this paper.

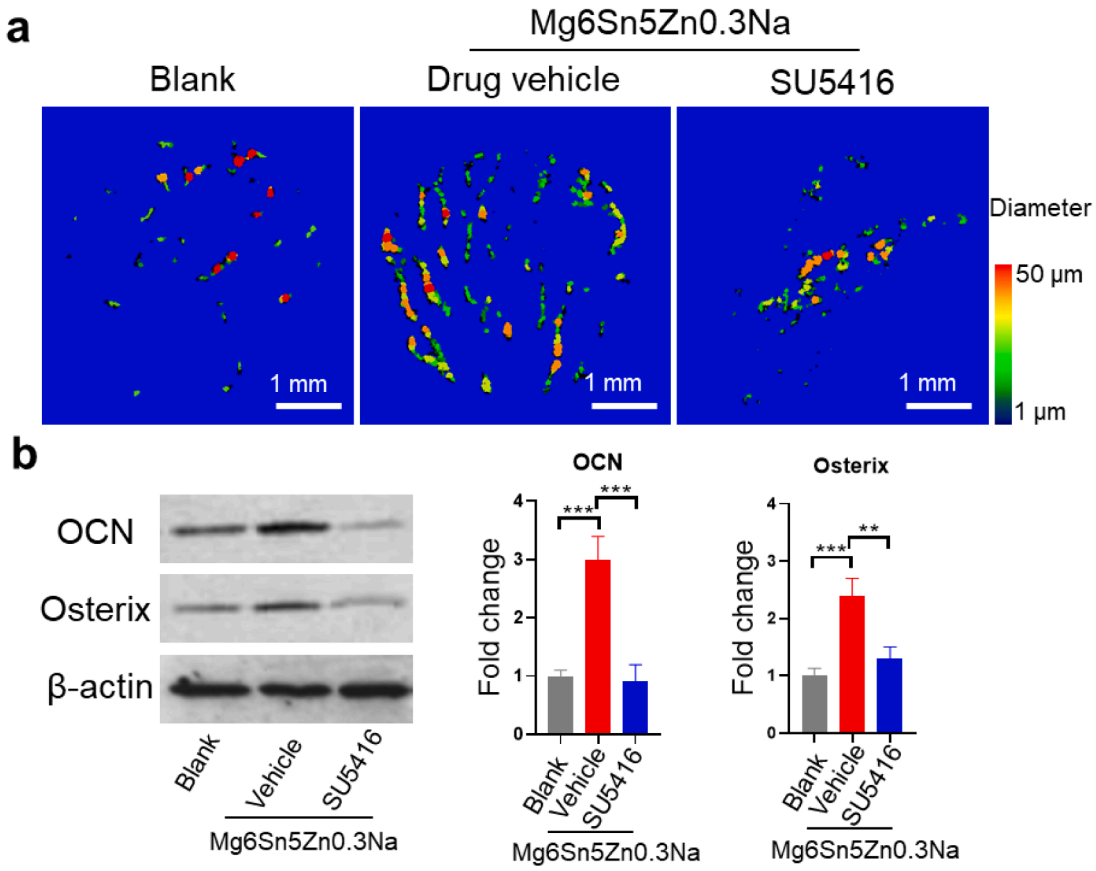

Fig. 8. Mg6Sn5Zn0.3Na enhanced calvarial defect repair through promoting angiogenesis. (a) micro-CT based angiography. Scale bar, 1 mm. (b) Western blotting for measuring the expression of OCN and Osterix in the defect region and the corresponding semi-quantitative data. **, $p < 0.01$. ***, $p < 0.001$. The reproducibility was validated in triple independent experiments.

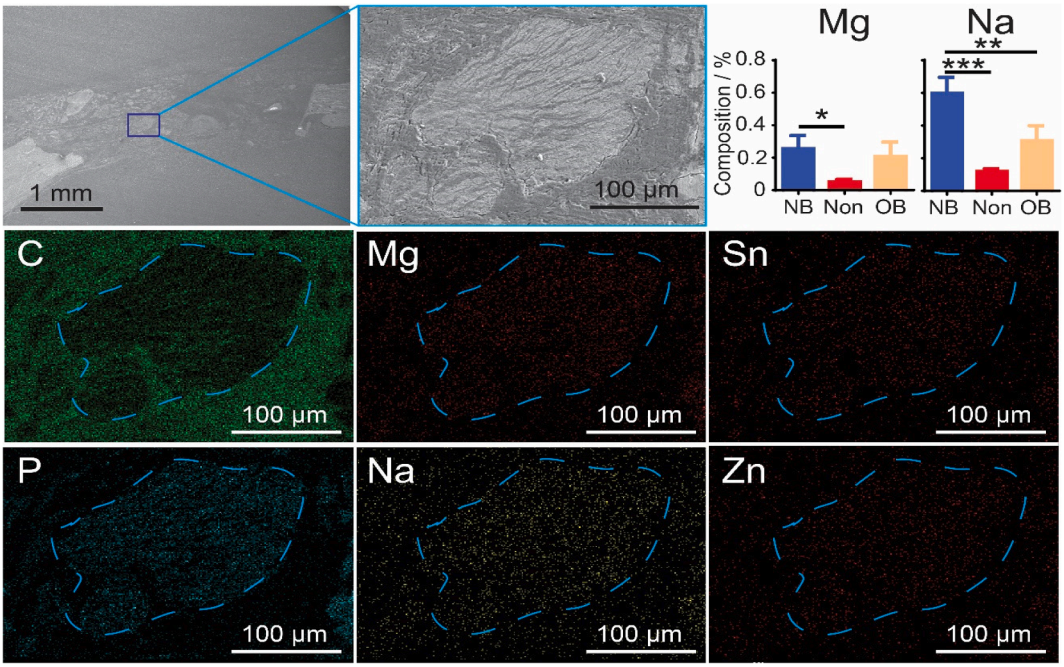

Fig. 9. Calvarial defect bone regeneration 12 weeks after implantation of Mg6Sn5Zn0.3Na scaffold. SEM image shows the cross-view of the whole defect with new bone formation inside, with the zoom-in image shows the morphology of region of interest (new bone) inside the defect. EDX mapping revealing the elemental distribution of C, P, Mg, Sn, Zn and Na. The composition of Mg and Na demonstrated the elemental concentration at different area from new bone inside the defect (NB), non-bone area inside the defect (Non) and old bone outside the defect (OB). The data (n = 3) were expressed as mean ± standard deviation (SD). *: $p < 0.05$, **: $p < 0.01$, and ***: $p < 0.001$.

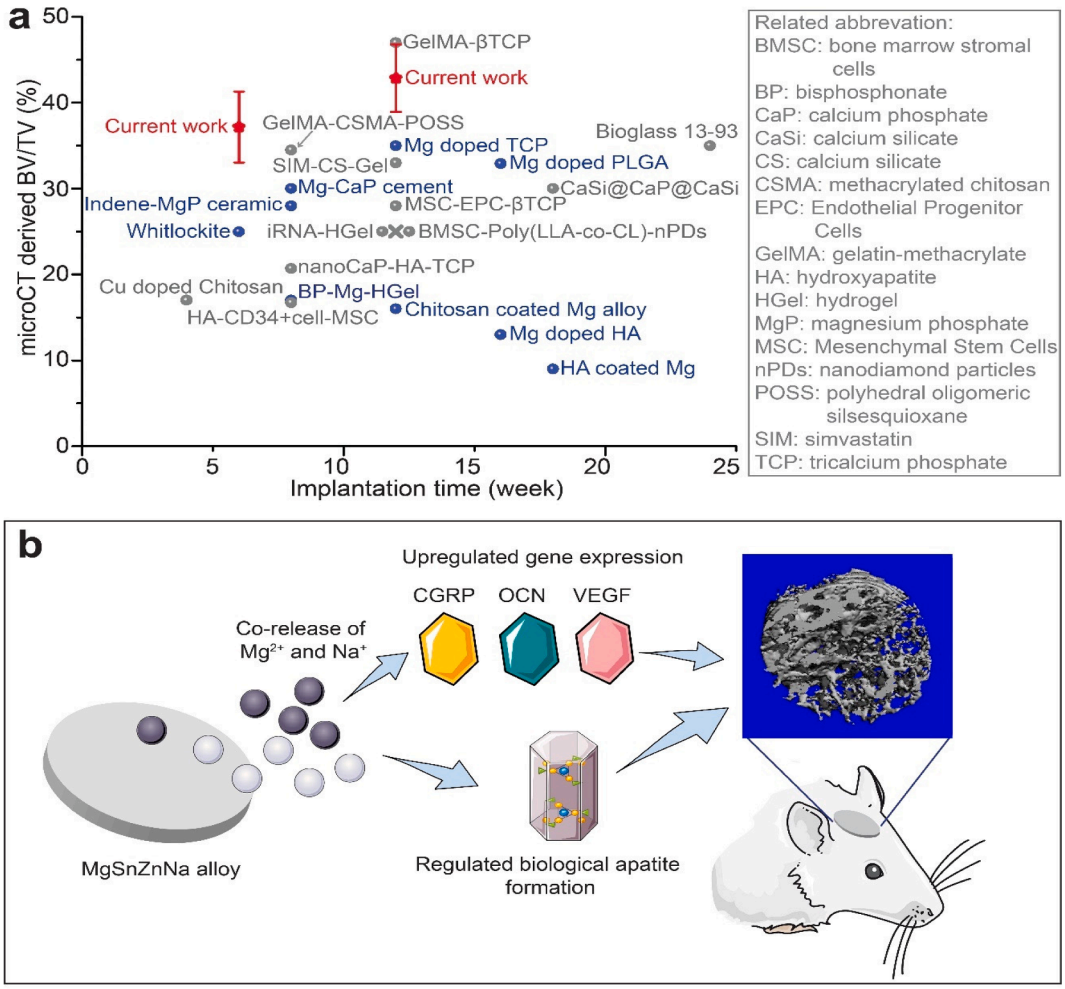

Fig. 10. a micro-CT derived bone mineralization (BV/TV) comparison between the present work (red), Mg-containing materials (blue) and ceramic and polymer -based materials (grey). b schematic illustration of the mechanism of MgSnZnNa alloy for enhanced bone regeneration. The co-release of Mg^{2+} and Na^{+} results in upregulated expression of CGRP and OCN *in vivo*, while in the meantime local Na helps regulate and optimize the structure of biological apatite.

Acknowledgements

We thank Prof. Matthew Barnett and Dr. Aiden Beer from Deakin University for the help in material preparation, and Ms Junyu Guo from University College London for the help on grammar, word use, and punctuation. This work was supported by National Natural Science Foundation of China, China [Grants No. 51871004, 31700819 and 81802152], NSFC/RGC Joint Research Scheme [Grant No. 5161101031], the Young Elite Scientists Sponsorship Program by CAST [YESS, Grant No. 2018QNRC001] and the Fundamental Research Funds for the Central Universities, China [Grant No. 06500098], the Hong Kong RGC Theme-based Research Scheme [Ref No. T13-402/17-N], RGC Collaborative Research Fund [Ref No. C4026-17WF].

References

[1] Y. Liu, Y. Zheng, X.-H. Chen, J.-A. Yang, H. Pan, D. Chen, L. Wang, J. Zhang, D. Zhu, S. Wu, K.W.K. Yeung, R.-C. Zeng, Y. Han, S. Guan, Fundamental theory of biodegradable metals—definition, criteria, and design, Adv. Funct. Mater. 29 (18) (2019) 1805402.

[2] C. Li, C. Guo, V. Fitzpatrick, A. Ibrahim, M.J. Zwierstra, P. Hanna, A. Lechtig, A. Nazarian, S.J. Lin, D.L. Kaplan, Design of biodegradable, implantable devices towards clinical translation, Nature Rev. Mater. (2019).

[3] Y. Zhang, J. Xu, Y.C. Ruan, M.K. Yu, M. O'Laughlin, H. Wise, D. Chen, L. Tian, D. Shi, J. Wang, S. Chen, J.Q. Feng, D.H. Chow, X. Xie, L. Zheng, L. Huang, S. Huang, K. Leung, N. Lu, L. Zhao, H. Li, D. Zhao, X. Guo, K. Chan, F. Witte, H. C. Chan, Y. Zheng, L. Qin, Implant-derived magnesium induces local neuronal production of CGRP to improve bone-fracture healing in rats, Nat. Med. 22 (10) (2016) 1160–1169.

[4] H. Windhagen, K. Radtke, A. Weizbauer, J. Diekmann, Y. Noll, U. Kreimeyer, R. Schavan, C. Stukenborg-Colsman, H. Waizy, Biodegradable magnesium-based screw clinically equivalent to titanium screw in hallux valgus surgery: short term results of the first prospective, randomized, controlled clinical pilot study, Biomed Eng Online 12 (2013) 62.

[5] J.W. Lee, H.S. Han, K.J. Han, J. Park, H. Jeon, M.R. Ok, H.K. Seok, J.P. Ahn, K. E. Lee, D.H. Lee, Long-term clinical study and multiscale analysis of in vivo biodegradation mechanism of Mg alloy, Proc. Natl. Acad. Sci. U.S.A. 113 (3) (2016).

[6] M. Schildwächter, BIOTRONIK Announces CE Mark for Magmaris, the First Clinically-Proven Bioresorbable Magnesium Scaffold, http://www.magmaris.com/en/newsroom/june-15-2016 (2016).

[7] D. Zhao, F. Witte, F. Lu, J. Wang, J. Li, L. Qin, Current status on clinical applications of magnesium-based orthopaedic implants: A review from clinical translational perspective, Biomaterials 112 (2017) 287–302.

[8] Y. Sun, H. Wu, W. Wang, R. Zan, H. Peng, S. Zhang, X. Zhang, Translational status of biomedical Mg devices in China, Bioactive Mater. 4 (2019) 358–365.

[9] G. Williams, N. Birbilis, H.N. McMurray, The source of hydrogen evolved from a magnesium anode, Electrochem. Commun. 36 (2013) 1–5.

[10] M. Esmaily, J.E. Svensson, S. Fajardo, N. Birbilis, G.S. Frankel, S. Virtanen, R. Arrabal, S. Thomas, L.G. Johansson, Fundamentals and advances in magnesium alloy corrosion, Prog. Mater. Sci. 89 (2017) 92–193.

[11] M. Cihova, P. Schmutz, R. Schäublin, J.F. Löffler, Biocorrosion zoomed in: evidence for dealloying of nanometric intermetallic particles in magnesium alloys, Adv. Mater. 31(42) (2019) 1903080.

[12] A. Myrissa, S. Braeuer, E. Martinelli, R. Willumeit-Römer, W. Goessler, A. M. Weinberg, Gadolinium accumulation in organs of Sprague–Dawley® rats after implantation of a biodegradable magnesium-gadolinium alloy, Acta Biomater (2016).

[13] N. Angrisani, J. Reifenrath, F. Zimmermann, R. Eifler, A. Meyer-Lindenberg, K. Vano-Herrera, C. Vogt, Biocompatibility and degradation of LAE442-based magnesium alloys after implantation of up to 3.5 years in a rabbit model, Acta Biomater. 44 (2016) 355–365.

[14] J. Emsley, Nature's Building Blocks: An A-Z Guide to the Elements, Oxford University Press, 2011.
[15] S.M. Barinov, Calcium phosphate-based ceramic and composite materials for medicine, Russian Chem. Rev. 79 (1) (2010) 13.
[16] J. Seong, W. Kim, Development of biodegradable Mg–Ca alloy sheets with enhanced strength and corrosion properties through the refinement and uniform dispersion of the Mg 2 Ca phase by high-ratio differential speed rolling, Acta Biomater. 11 (2015) 531–542.
[17] W. Morrison, Overview of microalloying in steel, The proceedings of the vanitec symposium, Guilin, China, 2000, pp. 25-35.
[18] H. Jin, S. Zhao, R. Guillory, P.K. Bowen, Z. Yin, A. Griebel, J. Schaffer, E.J. Earley, J. Goldman, J.W. Drelich, Novel high-strength, low-alloys Zn-Mg (<0.1wt% Mg) and their arterial biodegradation, Mater. Sci. Eng., C 84 (2018) 67–79.
[19] Z.-Z. Shi, J. Yu, X.-F. Liu, Microalloyed Zn-Mn alloys: from extremely brittle to extraordinarily ductile at room temperature, Mater. Des. 144 (2018) 343–352.
[20] S. Sun, Y. Ren, L. Wang, B. Yang, H. Li, G. Qin, Abnormal effect of Mn addition on the mechanical properties of as-extruded Zn alloys, Mater. Sci. Eng., A 701 (2017) 129–133.
[21] Y. Zhang, Y. Lu, X. Xu, L. Chen, T. Xiao, X. Luo, Y. Yan, D. Li, Y. Dai, K. Yu, Microstructure, corrosion behaviors in different simulated body fluids and cytotoxicity of Zn–Li alloy as biodegradable material, Mater. Trans. 60 (4) (2019) 583–586.
[22] J. Sangster, C.W. Bale, The Na-Sn (sodium-tin) system, J. Phase Equilibria Diffusion 19 (1) (1998) 76–81.
[23] C. Zhao, F. Pan, S. Zhao, H. Pan, K. Song, A. Tang, Preparation and characterization of as-extruded Mg–Sn alloys for orthopedic applications, Mater. Des. 70 (2015) 60–67.
[24] C. Zhao, F. Pan, S. Zhao, H. Pan, K. Song, A. Tang, Microstructure, corrosion behavior and cytotoxicity of biodegradable Mg–Sn implant alloys prepared by sub-rapid solidification, Mater. Sci. Eng., C 54 (2015) 245–251.
[25] J. Kubásek, D. Vojtěch, J. Lipov, T. Ruml, Structure, mechanical properties, corrosion behavior and cytotoxicity of biodegradable Mg–X (X = Sn, Ga, In) alloys, Mater. Sci. Eng., C 33 (4) (2013) 2421–2432.
[26] X. Gu, Y. Zheng, Y. Cheng, S. Zhong, T. Xi, In vitro corrosion and biocompatibility of binary magnesium alloys, Biomaterials 30 (4) (2009) 484–498.
[27] X. Lyu, Z. Yu, G. Wang, Biology of Elements (in Chinese), Press of University of Science and Technology of China, 2011.
[28] S. Zhang, X. Zhang, C. Zhao, J. Li, Y. Song, C. Xie, H. Tao, Y. Zhang, Y. He, Y. Jiang, Research on an Mg-Zn alloy as a degradable biomaterial, Acta Biomater. 6 (2) (2010) 626.
[29] H. Yang, X. Qu, W. Lin, C. Wang, D. Zhu, K. Dai, Y. Zheng, In vitro and in vivo studies on zinc-hydroxyapatite composites as novel biodegradable metal matrix composite for orthopedic applications, Acta Biomater. 71 (2018) 200–214.
[30] J.R. TerBush, N. Stanford, J.-F. Nie, M.R. Barnett, Na partitioning during thermomechanical processing of an Mg-Sn-Zn-Na alloy, Metallurgical Mater. Trans. A 44 (11) (2013) 5216–5225.
[31] J. Fischer, M.H. Prosenc, M. Wolff, N. Hort, R. Willumeit, F. Feyerabend, Interference of magnesium corrosion with tetrazolium-based cytotoxicity assays, Acta Biomater. 6 (5) (2010) 1813–1823.
[32] P.P. Spicer, J.D. Kretlow, S. Young, J.A. Jansen, F.K. Kasper, A.G. Mikos, Evaluation of bone regeneration using the rat critical size calvarial defect, Nat. Protoc. 7 (10) (2012) 1918–1929.
[33] Y. Liu, X. Liu, Z. Zhang, N. Farrell, D. Chen, Y. Zheng, Comparative, real-time in situ monitoring of galvanic corrosion in Mg-Mg2Ca and Mg-MgZn2 couples in Hank's solution, Corros. Sci. 161 (2019), 108185.
[34] J. Meng, W. Sun, Z. Tian, X. Qiu, D. Zhang, Corrosion performance of magnesium (Mg) alloys containing rare-earth (RE) elements, Corrosion Prevention of Magnesium Alloys, Elsevier2013, pp. 38-60.
[35] Y. Zong, G. Yuan, X. Zhang, L. Mao, J. Niu, W. Ding, Comparison of biodegradable behaviors of AZ31 and Mg–Nd–Zn–Zr alloys in Hank's physiological solution, Mater. Sci. Eng., B 177 (5) (2012) 395–401.
[36] Y. Ebisawa, T. Kokubo, K. Ohura, T. Yamamuro, Bioactivity of CaO·SiO2-based glasses: in vitro evaluation, J. Mater. Sci. – Mater. Med. 1 (4) (1990) 239–244.
[37] K. Ohura, T. Nakamura, T. Yamamuro, Y. Ebisawa, T. Kokubo, Y. Kotoura, M. Oka, Bioactivity of CaO·SiO2 glasses added with various ions, J. Mater. Sci. – Mater. Med. 3 (2) (1992) 95–100.
[38] F. Tamimi, D.L. Nihouannen, D.C. Bassett, S. Ibasco, U. Gbureck, J. Knowles, A. Wright, A. Flynn, S.V. Komarova, J.E. Barralet, Biocompatibility of magnesium phosphate minerals and their stability under physiological conditions, Acta Biomater. 7 (6) (2011) 2678–2685.
[39] J. Mi, J. Xu, H. Yao, X. Li, W. Tong, Y. Li, B. Dai, X. He, D.H.K. Chow, G. Li, Calcitonin gene-related peptide enhances distraction osteogenesis by increasing angiogenesis, Tissue Eng. (ja) (2020).
[40] K. Zhang, S. Lin, Q. Feng, C. Dong, Y. Yang, G. Li, L. Bian, Nanocomposite hydrogels stabilized by self-assembled multivalent bisphosphonate-magnesium nanoparticles mediate sustained release of magnesium ion and promote in-situ bone regeneration, Acta Biomater. 64 (2017) 389–400.
[41] J. Zhang, X. Ma, D. Lin, H. Shi, Y. Yuan, W. Tang, H. Zhou, H. Guo, J. Qian, C. Liu, Magnesium modification of a calcium phosphate cement alters bone marrow stromal cell behavior via an integrin-mediated mechanism, Biomaterials 53 (2015) 251–264.
[42] Z. Yuan, P. Wei, Y. Huang, W. Zhang, F. Chen, X. Zhang, J. Mao, D. Chen, Q. Cai, X. Yang, Injectable PLGA microspheres with tunable magnesium ion release for promoting bone regeneration, Acta Biomater. 85 (2019) 294–309.
[43] T. Xu, X. He, Z. Chen, L. He, M. Lu, J. Ge, J. Weng, Y. Mu, K. Duan, Effect of magnesium particle fraction on osteoinduction of hydroxyapatite sphere-based scaffolds, J. Mater. Chem. B 7 (37) (2019) 5648–5660.
[44] H. Shao, A. Liu, X. Ke, M. Sun, Y. He, X. Yang, J. Fu, L. Zhang, G. Yang, Y. Liu, S. Xu, Z. Gou, 3D robocasting magnesium-doped wollastonite/TCP bioceramic scaffolds with improved bone regeneration capacity in critical sized calvarial defects, J. Mater. Chem. B 5 (16) (2017) 2941–2951.
[45] J.A. Kim, H.S. Yun, Y.A. Choi, J.E. Kim, S.Y. Choi, T.G. Kwon, Y.K. Kim, T.Y. Kwon, M.A. Bae, N.J. Kim, Y.C. Bae, H.I. Shin, E.K. Park, Magnesium phosphate ceramics incorporating a novel indene compound promote osteoblast differentiation in vitro and bone regeneration in vivo, Biomaterials 157 (2018) 51–61.
[46] H.L. Jang, G.B. Zheng, J. Park, H.D. Kim, H.R. Baek, H.K. Lee, K. Lee, H.N. Han, C. K. Lee, N.S. Hwang, J.H. Lee, K.T. Nam, In vitro and in vivo evaluation of whitlockite biocompatibility: comparative study with hydroxyapatite and beta-tricalcium phosphate, Adv. Healthc. Mater. 5 (1) (2016) 128–136.
[47] Y. Guo, Y. Yu, L. Han, S. Ma, J. Zhao, H. Chen, Z. Yang, F. Zhang, Y. Xia, Y. Zhou, Biocompatibility and osteogenic activity of guided bone regeneration membrane based on chitosan-coated magnesium alloy, Mater. Sci. Eng. C, Mater. Biol. Applications 100 (2019) 226–235.
[48] S.H. Byun, H.K. Lim, S.M. Kim, S.M. Lee, H.E. Kim, J.H. Lee, The bioresorption and guided bone regeneration of absorbable hydroxyapatite-coated magnesium mesh, J. Craniofac. Surg. 28 (2) (2017) 518–523.
[49] X. Liu, M.N. Rahaman, Q. Fu, Bone regeneration in strong porous bioactive glass (13–93) scaffolds with an oriented microstructure implanted in rat calvarial defects, Acta Biomater. 9 (1) (2013) 4889–4898.
[50] G. Li, X. Wang, J. Cao, Z. Ju, D. Ma, Y. Liu, J. Zhang, Coculture of peripheral blood CD34+ cell and mesenchymal stem cell sheets increase the formation of bone in calvarial critical-size defects in rabbits, Br. J. Oral Maxillofac. Surg. 52 (2) (2014) 134–139.
[51] J. Zhang, H. Wang, J. Shi, Y. Wang, K. Lai, X. Yang, X. Chen, G. Yang, Combination of simvastatin, calcium silicate/gypsum, and gelatin and bone regeneration in rabbit calvarial defects, Sci. Rep. 6 (2016) 23422.
[52] M.A. Yassin, K. Mustafa, Z. Xing, Y. Sun, K.E. Fasmer, T. Waag, A. Krueger, D. Steinmuller-Nethl, A. Finne-Wistrand, K.N. Leknes, A copolymer scaffold functionalized with nanodiamond particles enhances osteogenic metabolic activity and bone regeneration, Macromol. Biosci. 17 (6) (2017).
[53] Y. Zhang, M. Chen, J. Tian, P. Gu, H. Cao, X. Fan, W. Zhang, In situ bone regeneration enabled by a biodegradable hybrid double-network hydrogel, Biomater. Sci. 7 (8) (2019) 3266–3276.
[54] S. D'Mello, S. Elangovan, L. Hong, R.D. Ross, D.R. Sumner, A.K. Salem, Incorporation of copper into chitosan scaffolds promotes bone regeneration in rat calvarial defects, J. Biomed. Mater. Res. Part B, Appl. Biomater. 103 (5) (2015) 1044–1049.
[55] D. Lee, E.J. Choi, S.E. Lee, K.L. Kang, H.-J. Moon, H.J. Kim, Y.H. Youn, D.N. Heo, S. J. Lee, H. Nah, Y.-S. Hwang, Y.-H. Lee, J. Seong, S.H. Do, I.K. Kwon, Injectable biodegradable gelatin-methacrylate/β-tricalcium phosphate composite for the repair of bone defects, Chem. Eng. J. 365 (2019) 30–39.
[56] H. Zigdon-Giladi, T. Bick, D. Lewinson, E.E. Machtei, Mesenchymal stem cells and endothelial progenitor cells stimulate bone regeneration and mineral density, J. Periodontol. 85 (7) (2014) 984–990.
[57] A. Xu, C. Zhuang, S. Xu, F. He, L. Xie, X. Yang, Z. Gou, Optimized bone regeneration in calvarial bone defect based on biodegradation-tailoring dual-shell biphasic bioactive ceramic microspheres, Sci. Rep. 8 (1) (2018) 3385.
[58] M.K. Nguyen, O. Jeon, P.N. Dang, C.T. Huynh, D. Varghai, H. Riazi, A. McMillan, S. Herberg, E. Alsberg, RNA interfering molecule delivery from in situ forming biodegradable hydrogels for enhancement of bone formation in rat calvarial bone defects, Acta Biomater. 75 (2018) 105–114.
[59] P. Pripatnanont, P. Praserttham, S. Suttapreyasri, N. Leepong, N. Monmaturapoj, Bone regeneration potential of biphasic nanocalcium phosphate with high hydroxyapatite/tricalcium phosphate ratios in rabbit calvarial defects, Int. J. Oral Maxillofac. Implants 31 (2) (2016).
[60] W. Yu, R. Li, J. Long, P. Chen, A. Hou, L. Li, X. Sun, G. Zheng, H. Meng, Y. Wang, A. Wang, X. Sui, Q. Guo, S. Tao, J. Peng, L. Qin, S. Lu, Y. Lai, Use of a three-dimensional printed polylactide-coglycolide/tricalcium phosphate composite scaffold incorporating magnesium powder to enhance bone defect repair in rabbits, J. Orthopaedic Translation 16 (2019) 62–70.
[61] S. Chen, P. Wan, B. Zhang, K. Yang, Y. Li, Facile fabrication of the zoledronate-incorporated coating on magnesium alloy for orthopaedic implants, J. Orthopaedic Translation (2019).
[62] B. Song, W. Li, Z. Chen, G. Fu, C. Li, W. Liu, Y. Li, L. Qin, Y. Ding, Biomechanical comparison of pure magnesium interference screw and polylactic acid polymer interference screw in anterior cruciate ligament reconstruction—a cadaveric experimental study, J. Orthopaedic Translation 8 (2017) 32–39.
[63] M. Yamaguchi, Role of zinc in bone formation and bone resorption, J. Trace Elements Exp. Med. 11 (2–3) (1998) 119–135.
[64] A.M. Arnold, B.D. Holt, L. Daneshmandi, C.T. Laurencin, S.A. Sydlik, Phosphate graphene as an intrinsically osteoinductive scaffold for stem cell-driven bone regeneration, Proc. Natl. Acad. Sci. 116 (11) (2019) 4855–4860.
[65] H.S. Han, I. Jun, H.K. Seok, K.S. Lee, K. Lee, F. Witte, D. Mantovani, Y.C. Kim, S. Glyn-Jones, J.R. Edwards, Biodegradable magnesium alloys promote angio-osteogenesis to enhance bone repair, Adv. Sci. 7 (15) (2020) 2000800.
[66] M.E. Fleet, X. Liu, Coupled substitution of type A and B carbonate in sodium-bearing apatite, Biomaterials 28 (6) (2007) 916–926.
[67] J.A. Rincón-López, J.A. Hermann-Muñoz, N. Cinca-Luis, B. Garrido-Domiguez, I. García-Cano, J.M. Guilemany-Casadamon, J.M. Alvarado-Orozco, J. Muñoz-Saldaña, Preferred growth orientation of apatite crystals on biological

hydroxyapatite enriched with bioactive glass: a biomimetic behavior, Cryst. Growth Des. 19 (9) (2019) 5005–5018.
[68] S. Peroos, Z. Du, N.H. de Leeuw, A computer modelling study of the uptake, structure and distribution of carbonate defects in hydroxy-apatite, Biomaterials 27 (9) (2006) 2150–2161.
[69] L. Lu, L. Wu, J. Chen, X. Lin, C. Wan, Q. Li, Effects of sodium on rat osteoblast and the role of epithelial sodium channel, J. Southern Med. Univ. 31 (11) (2011) 1871–1874.
[70] I. Ohsawa, M. Ishikawa, K. Takahashi, M. Watanabe, K. Nishimaki, K. Yamagata, K. I. Katsura, Y. Katayama, S. Asoh, S. Ohta, Hydrogen acts as a therapeutic antioxidant by selectively reducing cytotoxic oxygen radicals, Nat. Med. 13 (6) (2007) 688.
[71] J. Cai, Z. Kang, W.W. Liu, X. Luo, S. Qiang, J.H. Zhang, S. Ohta, X. Sun, W. Xu, H. Tao, R. Li, Hydrogen therapy reduces apoptosis in neonatal hypoxia–ischemia rat model, Neurosci. Lett. 441 (2) (2008) 167–172.
[72] H. Kawasaki, J. Guan, K. Tamama, Hydrogen gas treatment prolongs replicative lifespan of bone marrow multipotential stromal cells in vitro while preserving differentiation and paracrine potentials, BBRC 397 (3) (2010) 608–613.